analytical chemistry

pubs.acs.org/ac Article

Quantum Dot–Peptide Conjugates as Energy Transfer Probes for Sensing the Proteolytic Activity of Matrix Metalloproteinase-14

Zhicheng Jin, Narjes Dridi, Goutam Palui, Valle Palomo, Jesse V. Jokerst, Phillip E. Dawson, Qing-Xiang Amy Sang, and Hedi Mattoussi*

Cite This: *Anal. Chem.* 2023, 95, 2713–2722 Read Online

ACCESS | Metrics & More | Article Recommendations | Supporting Information

ABSTRACT: We detail the assembly and characterization of quantum dot (QD)–dye conjugates constructed using a peptide bridge specifically designed to recognize and interact with a breast cancer biomarker—matrix metalloproteinase-14 (MMP-14). The assembled QD conjugates are then used as optically addressable probes, relying on Förster resonance energy transfer (FRET) interactions as a transduction mechanism to detect the activity of MMP-14 in solution phase. The QDs were first coated with dithiolane poly(ethylene glycol) (PEG) bearing a carboxyl group that allows coupling via amide bond formation with different dye-labeled peptides. The analytical capability of the conjugates is enabled by correlating changes in the FRET efficiency with the conjugate valence and/or QD-to-dye separation distance, triggered and modulated by enzymatic proteolysis of surface-tethered peptides. The FRET probe exhibits great sensitivity to enzyme digestion with sub-nanomolar limit of detection. We further analyze the proteolysis data within the framework of the Michaelis–Menten model, which considers the fact that surface-attached peptides have a slower diffusion coefficient than free peptides. This results in reduced collision frequency and lower catalytic efficiency, k_{cat}/K_M. Our results suggest that our conjugate design is promising, effective, and potentially useful for *in vivo* analysis.

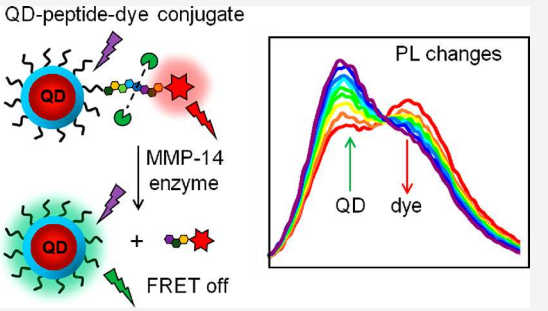

INTRODUCTION

Human membrane-type 1 matrix metalloproteinase, also commonly referred to as matrix metalloproteinase-14 (MMP-14), is known to promote cancer progression through hydrolysis of interstitial collagen, allowing tumor cells to escape and seed metastasis.[1−3] In addition, the upregulation of MMP-14 in breast cancer tissues has made this protease an important pharmaceutical target for tumor diagnosis and treatment.[2−4] Among the established diagnostic methods, fluorescence-based sensors, which often rely on changes in the fluorescence or Förster resonance energy transfer (FRET) interactions, as a signal transduction mechanism, have been actively explored.[4−8] FRET efficiency is highly sensitive to small changes in the donor–acceptor separation distance and is thus ideal for probing dimensions comparable to those of biomolecules. It has found widespread use in biosensing applications.[6,8,9]

Luminescent semiconductor nanocrystals (quantum dots, QDs) offer several unique spectroscopic features that can improve FRET efficiency and data analysis.[10−16] For example, the broad and tunable excitation bandwidth of QD donors allows one to reduce acceptor emission due to direct excitation, which can be achieved by exciting the pair at the valley of the acceptor absorbance profile. High photoluminescence quantum yields (PLQYs) combined with size-tunable emission of QDs allow for a maximized spectral overlap and therefore enhanced FRET interactions. In addition, their pronounced resistance to photobleaching ensures that samples can be monitored for extended periods of time. Lastly, given their large surfaces (compared to molecular dyes), each QD can be coupled to several acceptors, promoting strong FRET interactions. These key features have attracted much interest in developing QD-based conjugates for use in a wide range of biosensing applications.[16−21]

Assembling FRET-based nanoprobes that can find effective use in biological sensing requires high-quality biocompatible QDs that exhibit great colloidal and structural stability along with high PLQYs.[4,17−22] However, as-prepared highly fluorescing QDs are routinely grown under strictly hydrophobic conditions.[23−27] Several surface coating strategies relying, among others, on ligand substitution using coordinating poly(ethylene glycol) or zwitterion-rich motifs have been developed to interface the QDs with biological systems.[28−33] These surface coating methods ensure compact size, high PL, and long-term colloidal stability.[28,30,32−38] Subsequent bio-

Received: August 4, 2022
Accepted: December 29, 2022
Published: January 27, 2023

https://doi.org/10.1021/acs.analchem.2c03400
Anal. Chem. 2023, 95, 2713–2722

conjugation of PEGylated ligand-stabilized nanocrystals could be challenging nonetheless.[38−40] For example, metal−histidine coordination has been exploited by our group and others to facilitate the direct immobilization of polyhistidine-tagged peptides and proteins onto zinc-rich QD surfaces.[26,41,42] Although simple, this conjugation strategy is not effective in the presence of fully passivated nanocrystals using ligands that bind strongly and/or are not small enough.[41] Alternatively, integrating specific functionalities within the surface coating enables bio-orthogonal reactions to be implemented on the nanocrystals, yielding robust bioconjugates that preserve their structural integrity under a broad range of conditions.[37,43,44]

Here, we rely on a well-established conjugation method to assemble a set of QD−peptide conjugates as a FRET-based biosensor and validate that in the *in vitro* detection of the MMP-14 enzymatic activity. Core−shell CdSe−ZnS QDs were coated with dithiolane poly(ethylene glycol) (PEG) ligands bearing a terminal carboxyl group that allows amide bond formation with two sets of tetramethylrhodamine (TAMRA) dye-labeled peptides (a substrate sequence for MMP-14 and a control sequence). The TAMRA absorption profile exhibits a pronounced spectral overlap with the photoluminescence (PL) of green-emitting QDs (peak emission at 542 nm), making this donor−acceptor pair ideally suitable for probing FRET interactions. We utilize these conjugates to simultaneously track the time-dependent QD PL recovery and dye PL decay, which are attributed to changes in FRET interactions *via* interfacial enzyme proteolysis. We find that the QD−peptide can account for MMP-14 at sub-nanomolar concentrations. Quantitative evaluation of the kinetic data indicates a rather reduced catalytic efficiency for our sample configuration, where the substrate peptides are integrated within QD−peptide conjugates, compared to that measured for the freely diffusing biomolecules. We attribute this finding to, among others, a combination of slow substrate diffusion and crowding of surface-coupled QD−peptides.

EXPERIMENTAL SECTION

QD Surface Functionalization. Phase transfer and surface functionalization of CdSe−ZnS core−shell QDs were implemented using a rapid photoligation strategy, which relies on the in situ reduction and coordination of lipoic acid (LA) groups on the QD surfaces in a mixture of LA-PEG_{750}-OMe and LA-PEG_{600}-COOH ligands under UV irradiation.[37,43,45−47] Typically, ∼300 μL of as-grown hydrophobic QD dispersion (stock sample, 12.1 μM) was precipitated with 5 mL of ethanol and then centrifuged at 3500 rpm for 10 min. The resulting pellet was redispersed in hexane (750 μL) using a scintillation vial. Separately, a mixture of LA-PEG_{750}-OCH_3 (40.2 mg), LA-PEG_{600}-COOH (25.7 mg), and TMAH (1−3 mg) was dissolved in 500 μL of MeOH using an Eppendorf microtube. The ligand mixture was slowly added to the above QD dispersion. These conditions yield a ligand mixture with a molar ratio of LA-PEG_{750}-OCH_3:LA-PEG_{600}-COOH = 80:20 and a molar excess of total PEGylated ligand-to-QD of ∼20,000-to-1. A stir bar was introduced, and the vial was placed in a UV photoreactor (Luzchem UV lamp, model LZC-4 V) and irradiated with a UV flux centered at 350 nm for 30−40 min.[37,45] The QDs were precipitated by adding a mixture of $CHCl_3$ (∼500 μL) and hexane (∼5 mL) and then centrifuged at 3500 rpm for 5 min. The supernatant was discarded, and the yellowish pellet was redispersed in 500 μL of MeOH. Another round of precipitation was applied using a mixture of hexane and $CHCl_3$ as above, and the pellet was slightly dried and then dispersed in 4 mL of deionized (DI) water. The dispersion was passed through a syringe filter (PTFE, pore size ∼0.45 μm). Finally, the aqueous dispersion containing the carboxyl-modified QDs (QD-COOH) was further purified from excess free ligands by applying 3 rounds of concentration/dilution using a membrane filtration device (Millipore, with a cutoff M_W = 100 kDa), followed by storage at 4 °C until further use.[48]

Synthesis of Dye-Labeled Peptides. Here, we limit our description to the labeling of FS-6 peptides with maleimide−TAMRA. Briefly, 0.5 mg of FS-6 peptide was first dissolved in 300 μL of phosphate buffer (PB, pH 7.5, 20 mM); peptide concentration = 364 nM. Then, 0.3 mg (∼3 × molar excess with respect to peptide) of TCEP·HCl predissolved in 40 μL of PB was added to the peptide solution and stirred for 15 min at room temperature. Finally, 0.8 mg (4× molar excess with respect to peptide) of maleimide−TAMRA predissolved in DMSO (40 μL) was mixed with the peptide solution. The reaction was purged with N_2 and stirred at room temperature while protected from light exposure for 3 h. The reaction yield after HPLC purification was estimated at ∼90%.[49]

Assembly of QD-(Peptide-TAMRA)$_n$ Conjugates. Here, we limit our description to the assembly of QD-(FS-6-TAMRA)$_n$; other conjugates were formed using the same protocol. In a typical reaction, a 10 μL aliquot of QD-COOH dispersion (3.8 μM) was first diluted in PB buffer (20 mM, pH ∼ 7.5) to a final volume of 100 μL in a scintillation vial, and then 0.82 mg of EDC·HCl was dissolved in 20 μL of DI water at ∼1000× molar excess with respect to [-COOH], assuming that ∼80 -COOH per QD and NHS (0.12 mg in 20 μL of DI water at ∼250× molar excess with respect to [-COOH]) were added; the final dispersion pH was ∼5−6.5.[50,51] This yields a molar ratio of EDC/NHS = 4:1. The mixture was stirred at room temperature for 10 min to activate the surface carboxylic acid groups on the QD surfaces. Next, 100 μL of 20 mM PB (pH 10) was added to adjust the reaction medium to pH 8.[52] Finally, 15 μL of the TAMRA-labeled FS-6 peptide (80 μM in PB pH 7.5) was loaded, and the mixture was stirred at room temperature for 5 h while protected from light exposure. These conditions yield a molar ratio of peptide:QD ≈ 30:1. The final dispersion was passed through a PD-10 desalting column (GE Healthcare) to remove unreacted peptide−dye and excess coupling reagents, using a 50 mM kinetic buffer as the eluent. The elution was tracked using a hand-held UV lamp, and the first eluted band (yellow-color, ∼460 μL) was collected and stored at 4 °C for further use.

Proteolysis Assays. The recombinant cdMT1-MMP (catalytic domain of MT1-MMP or MMP-14, M_W ≈ 25 kDa) used in our study was kindly provided by Professor Harald Tschesche (Bielefeld University, Eastern Westphalia, Germany).[53] The stock solution of the purified and activated MMP-14 was aliquoted and stored at −80 °C in 50 mM 4-(2-hydroxyethyl)-1-piperazineethanesulfonic acid (HEPES), pH 7.5, 200 mM NaCl, 10 mM $CaCl_2$, 0.01% Brij-35, and 5% glycerol. Prior to use, each enzyme aliquot was thawed and diluted to the desired concentration using the kinetic buffer (50 mM HEPES, pH 7.5, 200 mM NaCl, 10 mM $CaCl_2$, 0.01% Brij-35). PL measurements to characterize the kinetic assays were carried out using an Infinite M1000 microplate reader (TECAN, Research Triangle Park, NC). Prior to incubation with the enzyme, 60 μL aliquots of the QD-(FS-6-TAMRA)$_{18}$ conjugates (at 18.5 nM) were preincubated with the desired

https://doi.org/10.1021/acs.analchem.2c03400
Anal. Chem. 2023, 95, 2713−2722

volumes of the 50 mM kinetic buffer in a 96-well microtiter plate at 27 °C for 50 min with intermittent 2 s mechanical shaking every 10 min until the PL signals reached equilibrium. Next, aliquots of MMP-14 stock (stock concentration ∼880 nM) at a volume ranging from 0 to 4.7 μL were rapidly pipetted into each well. Buffer was added to bring the total assay volume in each well to 80 μL and mixed thoroughly while avoiding air bubble generation. The fluorescence signal was then recorded every 10 min using a narrow excitation line at 380 nm for at least 4 h, and the emission spectra were simultaneously collected in the range of 515−680 nm. An intermittent 2 s mechanical shaking was employed after each round of PL data collection.

RESULTS AND DISCUSSION

Several groups including ours have explored the potential benefits (or limitations) of using fluorescent QDs as energy transfer donors and scaffolds for immobilizing several dye-labeled peptides as FRET conjugate substrates to characterize the proteolytic activity of soluble enzymes. Two configurations using, for example, a fixed enzyme concentration and varying the substrate concentration, or varying the enzyme concentration at a fixed substrate condition, focused on determining the Michaelis−Menten (MM) constant, K_M, the maximum velocity, v_{max}, and the limit of enzyme detection in these dispersion mixtures.[54,55] Other studies compared the rate of substrate digestion for the enzyme interacting with QD−peptide conjugates to the case of free substrates.[56] Those studies did not consider specific features corresponding to slower mobility and reduced collision frequency on the catalytic efficiency. We hereby tackle those questions using QD−peptide−dye conjugates interacting with MMP-14, an enzyme implicated in several diseases and with great pharmacological value, using a varying enzyme assay under fixed total substrate concentration in large excess. This study follows a recent study, where we used AuNP−peptide−dye conjugates, relying on dye quenching induced by plasmonic metal nanocrystals.[57]

Steady-state fluorescence measurements probing the interactions between luminescent QD donors and fluorescent dye acceptors, in dispersions of QD−peptide/protein−dye conjugates, have yielded pronounced QD PL quenching coupled with dye PL enhancement due to nonradiative QD→dye energy transfer interactions.[13,19,58] The process can be described within the Förster dipole−dipole interactions (or simply FRET) model.[59] The resulting changes in emission intensities can be used to extract a measure for the FRET efficiency (E_{FRET}) using

$$E_{FRET} = 1 - \frac{PL_{DA}}{PL_D} \quad (1)$$

where PL_D and PL_{DA}, respectively, designate the deconvoluted PL intensity of the donor alone and donor interacting with the proximal acceptors. For a centrosymmetric conjugate configuration with a single donor surrounded by n acceptors arrayed around the QD at a fixed average separation distance, r, the efficiency is expressed as[13,19]

$$E_{FRET} = \frac{nR_0^6}{nR_0^6 + r^6} \quad (2)$$

where R_0 is the Förster distance/radius corresponding to E_{FRET} = 50%.

When the peptide bridge in the QD−dye assembly is specifically recognized by a target enzyme for interactions, proteolysis would release several dye-labeled peptide fragments away from the QDs, lowering the energy transfer efficiency and producing QD PL recovery combined with a reduction in dye emission, as schematically represented in Figure 1. Analysis of the time- and concentration-dependent changes in the FRET efficiencies provides information about the kinetics of the catalytic proteolysis of the enzyme.[4,54,55,60]

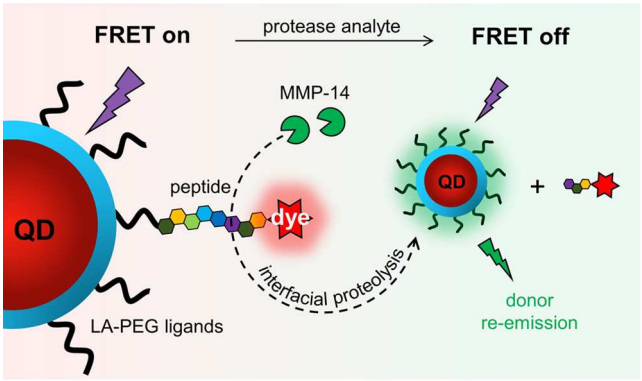

Figure 1. Schematic representation of a QD−peptide−dye conjugate along with the sensing configuration targeting the MMP-14 protease activity. The photoluminescence of the excited QDs is initially reduced due to energy transfer interaction (i.e., FRET on) but increases upon incubation with MMP-14 due to peptide cleavage and loss of FRET interactions (i.e., FRET off).

Assembly of the QD−Peptide Conjugate FRET Sensor. Two sets of bioconjugates were prepared comprising green-emitting QDs with a λ_{em} peak at 542 nm (542 nm QDs) and TAMRA dye assembled using an FS-6 or FS-6* peptide (see Table 1 and Figure S1). Hydrophobic QDs were first

Table 1. Peptide Information[a]

peptide	sequence	M_W (g mol^{-1})	protease
FS-6	H_2N-GGRPLG↓LYARAACA-$CONH_2$	1373.7	MMP-14
FS-6*	H_2N-ggrplglyaraaca-$CONH_2$	1373.7	N/A

[a]Note: H_2N-surface coupling site; G and A-spacer; ↓-enzyme recognition site; C-dye coupling site.

surface-functionalized with a mixture of LA-PEG_{750}-OCH_3 and LA-PEG_{600}-COOH (referred to as LA-PEG-OCH_3 and LA-PEG-COOH) at a molar ratio of 5:1, following previous protocols;[37,43,45] ^{1}H NMR spectra of the ligands are provided in the Supporting Information, Figure S1. This yielded hydrophilic QDs, where 20% of the total numbers of surface ligands, present carboxyl groups, which will be referred to as QD-COOH; the spatial extension of the PEG ligands is estimated to be ∼1.80 nm.[61] Figure 2a,b shows that a sizable spectral overlap between the QD PL and TAMRA absorption is achieved, with an overlap integral $I = 4.56 \times 10^{-13}$ M^{-1} cm^3. Table 1 shows the structures of two peptides; one substrate is designed to contain a sequence that is recognized by MMP-14 and the other sequence has no specific interactions with MMP-14 (i.e., control sequence).[62,63] Importantly, the peptide FS-6 has a modular structure, which includes (i) an N-terminal

https://doi.org/10.1021/acs.analchem.2c03400
Anal. Chem. 2023, 95, 2713−2722

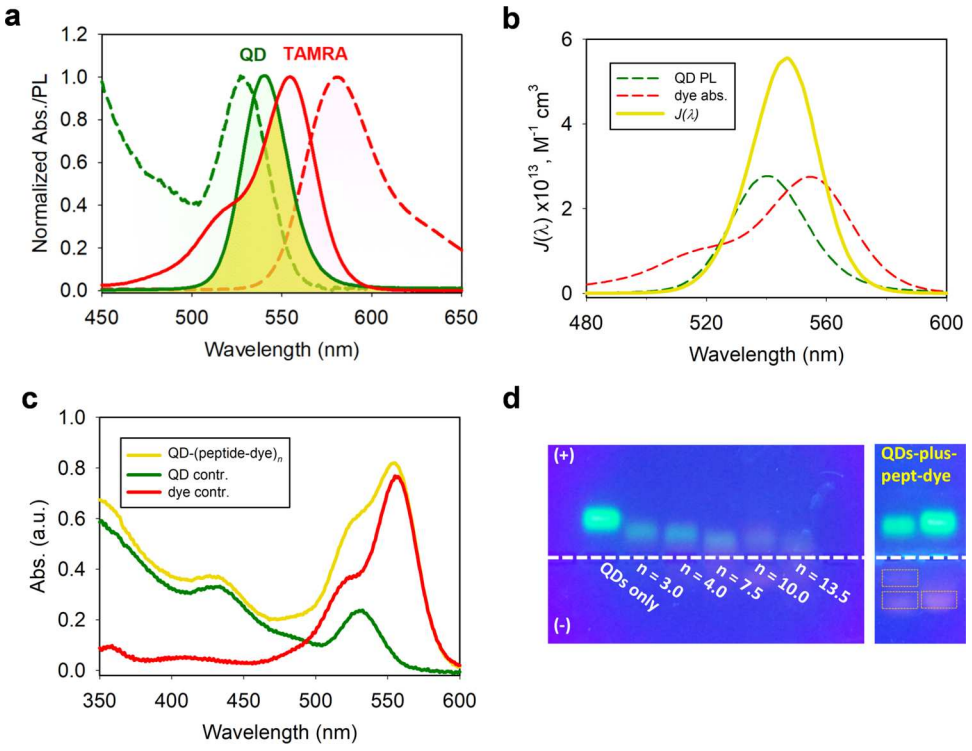

Figure 2. (a) Normalized spectra of the QD donor absorption (dashed green line), QD emission (solid green line), TAMRA absorption (solid red line), TAMRA emission (dashed red line), along with the spectral overlap region shown in yellow. (b) Spectral overlap function, $J(\lambda) = PL_{D\text{-}corr}(\lambda) \times \lambda^4 \times \varepsilon_A(\lambda)$, was calculated from the normalized profiles of donor emission and acceptor absorbance and used to extract a value for the spectral overlap integral, I, using (eq S3). (c) Deconvolution of the absorbance spectrum acquired from the QD-(peptide-TAMRA)$_n$ conjugates (yellow curve) yields contributions from the QDs (green line) and dye (red line). The conjugate valence, n, is extracted using the known molar absorption coefficients. (d) Gel electrophoresis image acquired under UV light from the PEGylated QD-COOH (QDs only band) side-by-side with the polyvalent QD-(peptide-TAMRA)$_n$ assemblies with increasing average valence, n (as noted); concentration = 75 nM. The dashed white line designates the loading wells, while "+" and "−" indicate the cathode and anode, respectively. Progressive reduction in the mobility shift is measured as more peptides are coupled to the QDs. The additional image shows that when mixtures of QDs and dye−peptide were loaded (left band: mixed overnight; right band: freshly mixed), independent and opposite mobility shifts were measured for the QD-COOH and dye−peptide (two dashed boxes designate hydrolyzed and intact maleimide rings). The 0.7% gel was run at 6.5 V cm^{-1} for 45 min.

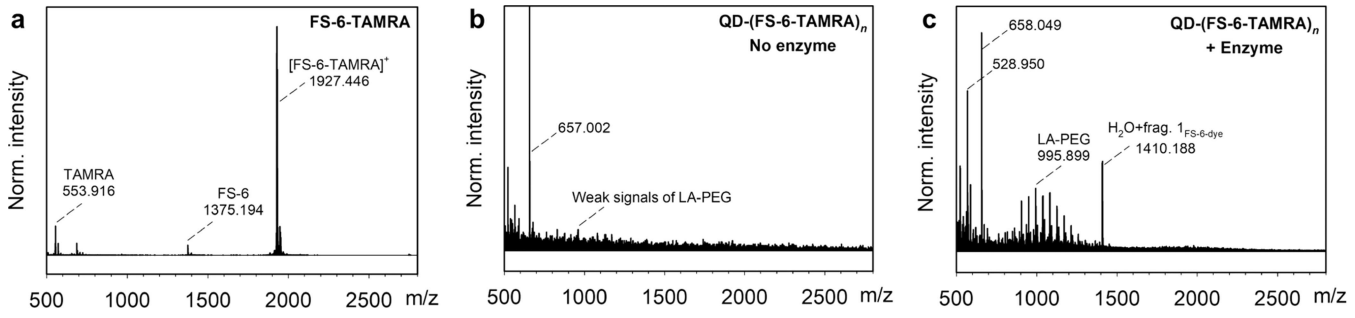

Figure 3. MALDI-TOF mass spectra of (a) TAMRA dye-labeled FS-6 peptide, (b) QD-(FS-6-TAMRA)$_n$ conjugate, showing a negligible PEG ligand signal with no detectable uncoupled peptide−dye after size exclusion chromatography, and (c) conjugate signature after the reaction with MMP-14 enzyme, showing a dye-labeled fragment. This proves that substrate proteolysis occurred on the QD surfaces.

amine for coupling to the QDs; (ii) a spacer consisting of repeating glycine (G) and alanine (A) residues for improving the protease accessibility; (iii) an MMP-14 cleavage site; (iv) a cysteine (C) for dye labeling;[22,64] and (v) an amidated C-terminus to eliminate secondary reactions. The control peptide (FS-6*) has the same sequence but is made of D-enantiomers.

The QD−peptide−dye conjugates were formed by coupling the TAMRA-labeled peptide to the fraction of reactive PEG−COOH surface ligands. The peptide−dye was first synthesized via maleimide-to-cysteine coupling by reacting the maleimide−TAMRA with the tris(2-carboxyethyl)phosphine (TCEP)-reduced peptide.[49] Next, the QD−peptide−dye conjugates (i.e., FRET pairs) were prepared by coupling the N-terminal amine of the peptide−dye to QD-COOH through the *N*-(3-dimethylaminopropyl)-*N*′-ethylcarbodiimide/*N*-hydroxysuccinimide (EDC/NHS) reaction. The optimal molar ratio of EDC-to-NHS that yielded the highest coupling efficiency was 4:1 (Figure S2). This result agrees with a previous report by Kanaras and co-workers.[40] Finally, PD-10 size exclusion column chromatography was applied to remove the uncoupled peptide−dye. Matrix-assisted laser desorption/ionization-time of flight (MALDI-TOF) mass spectrometry was used to

https://doi.org/10.1021/acs.analchem.2c03400
Anal. Chem. 2023, 95, 2713−2722

Table 2. Förster Resonance Energy Transfer (FRET) Parameters for the QD−TAMRA Pair

QD radius (Å)[24,65]	size of the ligand (Å)[61]	dye-labeled peptide	I ($M^{-1} \times cm^3$)	Förster radius, R_0 (Å)	D → A distance, r (Å)	peptide spatial extension (Å)
~30	~17.8	FS-6-TAMRA	4.56×10^{-13}	~50.8	~61.3 ± 1.9	~17.1−20.9

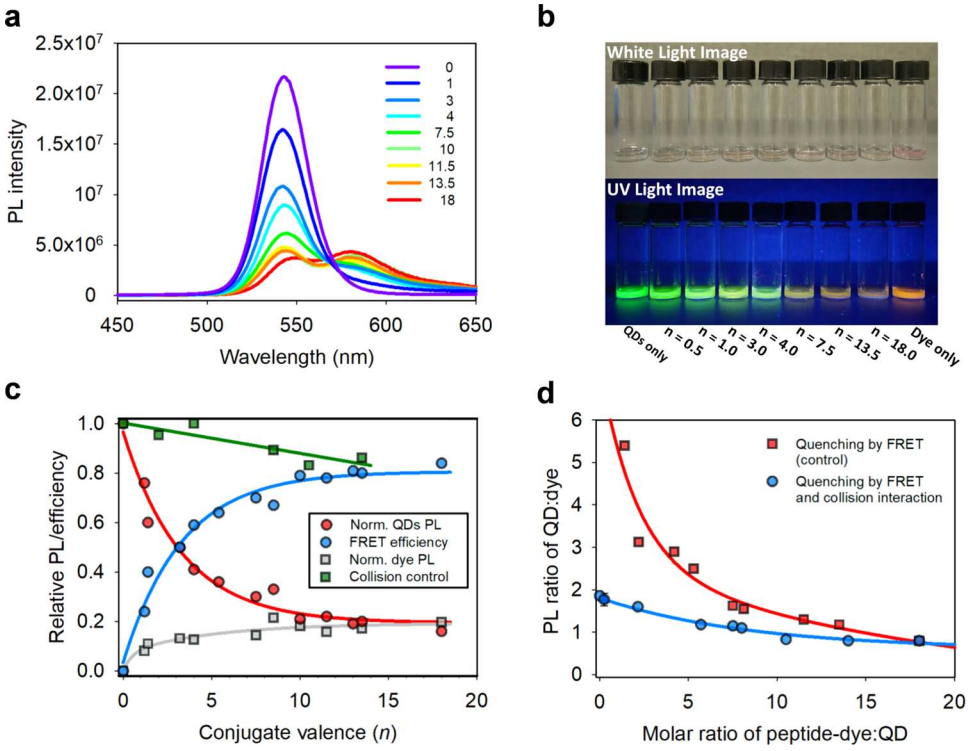

Figure 4. (a) Composite PL spectra measured for the QD-(FS-6-TAMRA)$_n$ with increasing valence. (b) White light image (top panel) and UV light image (bottom panel) taken of the QD−peptide−dye conjugates with an average valence number ranging from 0 to 18. The color change in the bottom panel is indicative of enhanced FRET interactions. (c) Normalized QD PL intensity measured after spectral deconvolution at each valence (red spheres); the corresponding FRET efficiency data are also shown (blue spheres). The control QD PL reduction due to collisional interactions collected from QDs mixed with various concentrations of free peptide−dye is also shown (green squares). The normalized TAMRA re-emission after spectral deconvolution is included (gray squares). (d) Standard curves of the ratio PL_{549}/PL_{581} vs conjugate valence for QD-(FS-6-TAMRA)$_{18}$. The red curve shows the PL of the conjugates only and accounts for FRET interactions. The blue curve, extracted from the PL of various mixtures of QD−dye and free peptide−dye, accounts for changes in the PL ratio induced by both FRET and collision interactions. The blue curve is fitted using an equation, with PL ratio = $1.854 - 1.719n/(9.529 + n)$.

confirm the dye−peptide coupling (Figure 3a). The technique was also used to acquire MS data from QD-COOH reacted with the TAMRA-labeled peptide, which showed that homogeneous conjugates have been formed (Figure 3b). Additionally, MS data acquired from the QD−peptide−dye conjugates that have been reacted with MMP-14 showed a well-defined signature (1410.188 m/z) ascribed to the digested TAMRA−peptide fragments, confirming that the QD-tethered peptides are recognized and digested by the enzyme (Figure 3c). This proves that the peptide stayed bioactive after dye attachment and tethering onto the QD surfaces.

Characterization of the FRET Sensor. We characterized the conjugates using UV−vis absorption and fluorescence spectroscopy. The composite absorption and fluorescence profiles acquired from the purified conjugates account for the effects of coupling multiple peptide−dye to a QD and the changes brought by FRET interactions. For example, the absorbance spectra acquired from the QD-(FS-6-TAMRA)$_n$ conjugates can be deconvoluted to isolate the characteristic QD and TAMRA contributions (e.g., see Figure 2c). The valence, n, designating the average dye-to-QD molar ratio in the polyvalent conjugates, is estimated by comparing the deconvoluted absorbance profiles to their respective molar absorption coefficients, namely, $\varepsilon_{350\,nm} = 8.1 \times 10^5\ M^{-1}\ cm^{-1}$ for QDs and $\varepsilon_{554\,nm} = 8.0 \times 10^4\ M^{-1}\ cm^{-1}$ for TAMRA in water.[22] Data indicate that the progressive increase in the dye absorption contribution to the composite profiles is commensurate with the equivalent peptide−dye introduced during the coupling reaction, proving that control over the conjugate valence has been realized. Docking several dye-labeled peptides around a QD as a means of enhancing FRET interactions has important implications for sensor performance, such as amplifying the signal output and improving sensitivity.[13,19,54,56]

The above absorption and fluorescence measurements were utilized to extract estimates for the energy transfer efficiency realized with these conjugates. We first calculated the spectral overlap integral, $I = 4.56 \times 10^{-13}\ M^{-1}\ cm^3$, and $R_0 \sim 5.1$ nm for the QD−TAMRA pair (see Figure 2b and Table 2). Figure 4a shows that the loss of QD emission (namely at 542 nm) tracks the increase in the valence n from 0 to 18. This also resulted in a bathochromic shift in the conjugate color when UV irradiated with a hand-held lamp (Figure 4b). FRET efficiency data deduced for the QD-(FS-6-TAMRA)$_n$ con-

https://doi.org/10.1021/acs.analchem.2c03400
Anal. Chem. 2023, 95, 2713−2722

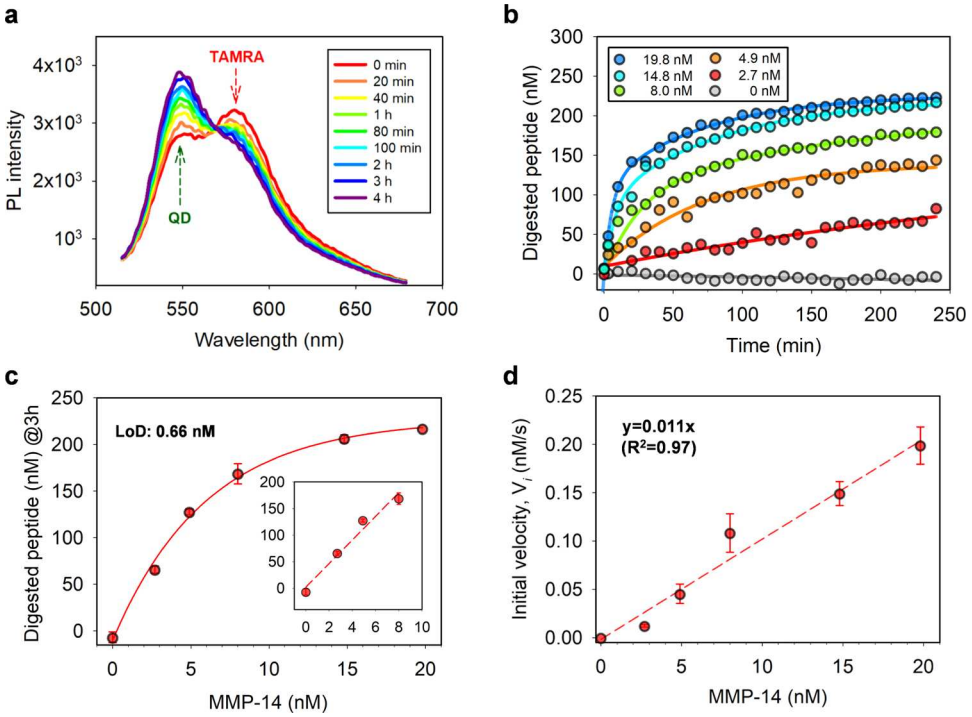

Figure 5. (a) Time-dependent progression of the conjugate PL during the proteolysis assay. 14 nM QD-(FS-6-TAMRA)$_{18}$ conjugates were incubated with 19.8 nM MMP-14. The composite PL spectra show enhancement in QD PL along with a decrease in sensitized TAMRA. (b) Time-dependent product formation measured upon incubation of QD-(FS-6-TAMRA)$_{18}$ conjugates with various enzyme concentrations. (c) Amount of digested peptide (at 3 h) in the conjugates as a function of MMP-14 concentration. The determined limit of detection (LoD) is 0.66 nM; the error bar represents the standard deviation (n = 2). (d) v_i vs [E] for the QD-(FS-6-TAMRA)$_{18}$ conjugates; [E] being the enzyme concentration. The initial velocity is extracted when [P] < [S]$_0$ × 15%. The data points are best fitted with the equation: $v_i = (k_{cat}[S]_0/K_M)\cdot[E]$.

jugates, as shown in Figure 4c, indicate that E_{FRET} reached 80–90% at n = 15. In comparison, less than 20% QD PL loss was measured for unconjugated QDs mixed with free peptide-TAMRA. They correspond to collisional quenching interactions (see Figure 4c, green squares). FRET analysis of the data shown in Figure 4 using eq 2 provided an estimate for the average center-to-center separation distance: $r \sim 6.1$ nm for QD-(FS-6-TAMRA)$_n$. This distance accounts for the spatial extension consisting of the QD radius (~3 nm, see TEM data in Figure S1), LA-PEG$_{600}$ ligand (~1.80 nm), and the inserted peptide (~1.7 nm), see Table 2.[24,61,65]

The above spectroscopic proof for the conjugate formation was further corroborated by gel electrophoresis measurements. Indeed, data on the gel mobility shift show that conjugates with increasing valence exhibit reduced mobility shift (toward the anode) compared to the shift measured for the starting QD-COOH, primarily due to the reduction of the negative charge combined with the overall increase in the conjugate size, brought by the tethering of several peptides that present positively charged arginine residues onto the QDs.[66] Additionally, the bands recorded for conjugates with high valence showed weak PL intensity due to strong FRET-induced quenching of QD PL. Two control samples made of QD-COOH mixed with free peptide–dye showed well-separated bands, ascribed to unconjugated QDs and peptide–dye (Figure 2d). These data also imply that nonspecific interactions between the LA-PEG-stabilized QDs and dye-labeled peptides are essentially negligible. Cumulatively, the gel mobility data confirm that conjugation of peptide–dye onto the QDs has taken place.

The FRET interactions and their exquisite dependence on the separation distance and/or conjugate valence, as reflected in data shown in Figure 4, are critically important for extracting information about the kinetics of enzyme proteolysis. Analysis of changes in the composite fluorescence profiles and the corresponding FRET efficiency data during proteolysis allow one to measure the amount of released TAMRA–peptide fragments from the conjugates during the digestion process, which can be further exploited to extract kinetic parameters. However, in our present case, we exploit changes in the PL ratio (i.e., the ratio of the PL peak values, PL_{549}/PL_{581}) instead of relying on E_{FRET} changes, to extract information about the enzyme proteolysis. This approach is more effective and provides easier to analyze data than using FRET efficiency data, as it accounts for changes in both donor and acceptor PL signals.[55,58] Figure 4d shows a plot of the ratio PL_{549}/PL_{581} acquired for the set of assembled QD-(FS-6-TAMRA)$_n$ conjugates. The profile of the PL ratio vs n shows a trend similar to that of QD PL loss vs n (see Figure 4, panels c vs d). It provides a standard curve for the spectroscopic response to increasing the QD–peptide-TAMRA conjugate valence n. However, analysis of the ratiometric data must consider that proteolysis cleaves a fraction of the peptide–dye, which reduces the actual valence of the remaining assemblies. They must also account for the fact that the displaced dye–peptide fragments still contribute to the QD PL quenching via solution-phase (collisional) quenching. To account for this, a newly corrected standard curve was experimentally generated by monitoring the ratiometric signal over a series of solution mixtures of QD-(FS-6-TAMRA)$_n$ with free FS-6–TAMRA while maintaining a constant QD-to-dye molar ratio; additional

https://doi.org/10.1021/acs.analchem.2c03400
Anal. Chem. 2023, 95, 2713–2722

details about how the corrected standard curve was assembled are provided in the Supporting Information. This standard curve was used in evaluating the amounts of cleaved peptides in the QD−peptide−dye conjugates during the proteolysis reaction.

Proteolytic Assays. Probing the kinetics of enzyme proteolysis under "varying substrate" conditions is challenging when using QD−peptide conjugates because that requires changing QD concentrations at a given conjugate valence, which complicates experimental implementation and data analysis.[16,54,67,68] Instead, we chose a "varying enzyme format" as an alternative condition, where effects of changes in the enzyme concentration while maintaining a fixed conjugate (and substrate) concentration are evaluated to characterize the enzyme proteolytic activity.[68−70] For this, we titrate varying molar amounts of the enzyme ($[E]_0$ = 0−19.8 nM) into the conjugate dispersion while maintaining a constant substrate concentration ($[S]_0$ = 260 nM) in all assays.[71] This concentration satisfies the condition of excess substrate and ensures a valid quasi-steady-state assumption (e.g., $[S]_0 > 10 \times [E]_0$).[72] Additional background details about the Michaelis−Menten kinetics are provided in the Supporting Information.

Figure 5a shows data acquired from a representative assay, where QD-$(FS\text{-}6\text{-}TAMRA)_{18}$ conjugates have been reacted with MMP-14 at a concentration of 19.8 nM. Progression of the composite fluorescence spectra shows enhancement in the QD PL (40−50% recovery) concomitant with a reduction in TAMRA emission. This accounts for reduction of the QD→TAMRA energy transfer interactions, triggered by MMP-14 cleavage of the peptide, resulting in reduced conjugate valence as well as FRET efficiency (eq 1). A similar trend was observed for another assay test using an enzyme concentration of 4.9 nM (Figure S3). The corresponding ratiometric PL data vs time acquired at various MMP-14 concentrations ranging from 0 to 19.8 nM are summarized in Figure S4. Notably, a shift in the color of the samples after proteolysis from orange to green could be visualized using a hand-held UV lamp. The time-dependent change in the composite fluorescence profiles has been converted to plots of time-dependent reaction products ([P] vs t) using the calibration curves discussed above, see Figure 5b.

Overall, the data in Figure 5a,b show two key features of the sensing construct described in this study. The fluorescence ratiometric data have a stable baseline, which proves that the conjugates are stable under the experimental conditions used. In addition, at least 85% of the surface-docked FS-6 peptides have reacted with the enzyme, resulting in proteolysis, which confirms that essentially all of the surface-tethered substrates are accessible to the enzyme. Also, no sign of macroscopic aggregation buildup after proteolysis has been observed. Figure 5c shows that the limit of detection (LoD) for MMP-14 is ∼0.66 nM for QD-$(FS\text{-}6\text{-}TAMRA)_{18}$.[73] Conversely, incubating the control QD-$(FS\text{-}6^*\text{-}TAMRA)_6$ conjugates with MMP-14 yielded no QD PL recovery over time (Figure S5). We have compared the data to those using the commercial fluorogenic substrates (e.g., SensoLyte 520), see reference (web link: https://www.anaspec.com/en/catalog/sensolyte-520-mmp-14-assay-kit-fluorimetric-1-kit~36d26810-0641-4879-90cd-3b84e4ffa469). Our limit of detection (∼ 0.66 nM) is slightly lower than the reported value (∼ 2 nM) using the fluorogenic substrates.

We now analyze the proteolysis data acquired using the varying enzyme assay format, within the Michaelis−Menten (MM) model under the standard quasi-steady-state assumption (sQSSA), where the concentration of enzyme-complexed substrate, [ES], stays constant. We extract values for the catalytic efficiency of MMP-14 measured using the two peptide-tethered on the QD surfaces and compare those to data reported in the literature using solutions of freely peptide substrate and MMP-14. The time-integrated MM equation under the sQSSA conditions yields a simple expression for the product buildup with time[63]

$$[P] = [S]_0 \cdot (1 - e^{-K_{obs} \cdot t}) \tag{3}$$

where the first-order rate constant K_{obs} is expressed as

$$K_{obs} = \frac{k_{cat}[E]}{K_M + [E]} \tag{4}$$

K_M is the MM constant defined as $K_M = ((k_{cat} + k_{off}))/k_{on}$. Equation 3 provides an easy fit to the experimental profiles for [P] vs t at each enzyme concentration, [E], as shown in Figure 5b. Additionally, applying the definition of the initial velocity to eq 3 yields

$$v_i = \left(\frac{d[P]}{dt}\right)_{t=0} = [S]_0 \cdot K_{obs} \tag{5}$$

v_i is extracted from the experimental digestion data limited to 15% substrate depletion. Equation 5 can further be simplified using the condition ($K_M \gg [E]$) to[63]

$$v_i \approx \frac{k_{cat}[S]_0}{K_M} \cdot [E] \tag{6}$$

This yields a simple linear relationship between the initial velocity and enzyme concentration, with a slope that is the product of the catalytic efficiency of the enzyme, k_{cat}/K_M, and $[S]_0$. Figure 5d shows that the experimental data for v_i vs [E] for the QD−peptide assemblies exhibit a linear trend as predicted by eq 6. Fitting the data combined with the use of the experimental value for $[S]_0$ = 260 nM yields an average value for k_{cat}/K_M = 36,500 M^{-1} s^{-1} for the QD-$(FS\text{-}6\text{-}TAMRA)_{18}$ substrates. Importantly, comparing this value to literature data extracted from assays employing soluble-free enzyme and peptide (i.e., k_{cat}/K_M = 1,253,000 M^{-1} s^{-1} for FS-6) indicates that the catalytic efficiency measured for our FRET conjugates is about two orders of magnitude smaller than the one reported using the free peptide.[62,63] The difference between the k_{cat}/K_M values measured using our polyvalent QD−peptide conjugates and those reported in the literature using solutions of peptides can be attributed to the effects of "substrate jamming" on the nanocrystal surfaces, which reduces the encounter frequency with the enzyme. Stringent steric constraints imposed by tethering the peptide substrates on the QD make it difficult to systematically describe the complex interfacial catalysis when the enzyme interacts with the surface-docked substrates.[74−76] Within these conditions, application of the classical Michaelis−Menten model has limited validity due to simplified assumptions relying on thermodynamically driven collisions between the enzyme and substrate in the absence of any colloid scaffold. Here, we briefly discuss and compare the interfacial catalysis and homogeneous proteolysis relying on diffusion−collision theory (see Figure S6a,b), as done for substrates tethered on Au nanoparticle (AuNP) surfaces.[57] The proposed rationale for explaining the reduced catalytic efficiency for a nano-

https://doi.org/10.1021/acs.analchem.2c03400
Anal. Chem. 2023, 95, 2713−2722

particle−peptide substrate (compared to interactions occurring in a homogeneous peptide solution) focuses on two physical factors: (i) the encounter frequency in a pairwise reaction is dictated by the molecule/species with the smaller molecular weight. Consequently, in a homogeneous solution involving soluble freely diffusing peptides and enzymes, the reaction rate depends on the diffusion properties of the smaller specimen, that is, the peptide. In our sample configuration, rather the QD conjugates constitute the larger solute objects, which would imply that the reaction rate is controlled by the diffusion coefficient of the soluble enzyme instead of the substrates. This in turn leads to a slower catalysis rate compared to the more conventional case of a homogeneous solution of enzyme-plus-peptide. (ii) The large nanoparticle size imposes stringent steric conditions that permit the enzyme to collide and react with the surface-tethered substrate (Figure S6c). This increases the frequency of "empty collisions" involving the enzyme interacting with the nonreactive regions of the QD conjugates. These aspects combined greatly lower the frequency of events producing enzyme−substrate complex formation and eventually yield a much smaller catalytic efficiency.

CONCLUSIONS

We constructed a set of colloidally stable QD-based FRET sensors *via* covalent peptide bond formation that are capable of probing the activity of the cancer biomarker MMP-14 with high sensitivity. Photoligation of hydrophobic QDs with terminally reactive PEG-appended lipoic acid provided conjugates with remarkable colloidal stability that is readily linked with peptide substrates. We characterized the conjugation by UV−vis absorption, steady-state emission, gel electrophoresis, and mass spectrometry. Our results proved successful surface immobilization and strong FRET interactions. The QD−peptide−dye conjugates were sensitive to MMP-14 at sub-nanomolar range (e.g., 0.66 nM). They also showed that up to 85% of surface-tethered substrates were hydrolyzed by the protease. We quantified the enzyme kinetics and extracted the estimate for the catalytic efficiency for this conjugate configuration. We further discussed our findings within the framework of the Michaelis−Menten kinetic model under the standard quasi-steady-state assumption (sQSSA), and found that the reduced mobility of QD-tethered substrates combined with steric effects reduce the encounter frequency between the free enzyme and surface-immobilized peptides. This results in decreased catalytic efficiency constant compared to freely diffusing biomolecules. The QD−peptide−dye conjugates exhibit high sensitivity to the enzyme, with a nanomolar range limit of detection achieved using our assay format. Overall, the data show the complexity of interfacial catalysis involving nanoparticle-conjugated substrates, which could be attributed to surface crowdedness, reduced collisions, and slow formation of ES complexes on solid nanosurfaces.

ASSOCIATED CONTENT

Supporting Information

The Supporting Information is available free of charge at https://pubs.acs.org/doi/10.1021/acs.analchem.2c03400.

Materials; instrumentation; methods; growth of QDs; TEM; ligand exchange; bioconjugation; gel electrophoresis; FRET background; and enzyme kinetics (PDF)

AUTHOR INFORMATION

Corresponding Author

Hedi Mattoussi − *Department of Chemistry and Biochemistry, Florida State University, Tallahassee, Florida 32306, United States;* orcid.org/0000-0002-6511-9323; Email: mattoussi@chem.fsu.edu

Authors

Zhicheng Jin − *Department of Chemistry and Biochemistry, Florida State University, Tallahassee, Florida 32306, United States;* Present Address: Department of NanoEngineering, University of California, San Diego, La Jolla, California 92093, United States; orcid.org/0000-0001-6072-7533

Narjes Dridi − *Department of Chemistry and Biochemistry, Florida State University, Tallahassee, Florida 32306, United States;* orcid.org/0000-0001-9267-5475

Goutam Palui − *Department of Chemistry and Biochemistry, Florida State University, Tallahassee, Florida 32306, United States;* Present Address: National Center for Toxicological Research, Food and Drug Administration, Jefferson, Arkansas 72079, United States.

Valle Palomo − *Department of Chemistry, The Scripps Research Institute, La Jolla, California 92037, United States;* Present Address: Department of Structural and Chemical Biology, Centro de Investigaciones Biológicas-CSIC, Madrid 28040, Spain; orcid.org/0000-0002-1473-4086

Jesse V. Jokerst − *Department of NanoEngineering, University of California, San Diego, La Jolla, California 92093, United States;* orcid.org/0000-0003-2829-6408

Phillip E. Dawson − *Department of Chemistry, The Scripps Research Institute, La Jolla, California 92037, United States;* orcid.org/0000-0002-2538-603X

Qing-Xiang Amy Sang − *Department of Chemistry and Biochemistry, Florida State University, Tallahassee, Florida 32306, United States;* orcid.org/0000-0001-8828-0569

Complete contact information is available at: https://pubs.acs.org/10.1021/acs.analchem.2c03400

Notes

The authors declare no competing financial interest.

ACKNOWLEDGMENTS

The authors thank FSU and the National Science Foundation (NSF-CHE, Grants #1508501 and #2005079), AFOSR (Grant No. FA9550-18-1-0144), and Kasei-Asahi Corporation for financial support. J.V.J. acknowledges the support from the NSF funding under award 1845683 and NIH funding under award P30 NS047101. They also thank Dr. Hong Li, Margaret Seavy, and Yizhuang Tong for the fruitful discussions on material purification and kinetic study.

REFERENCES

(1) Zarrabi, K.; Dufour, A.; Li, J.; Kuscu, C.; Pulkoski-Gross, A.; Zhi, J.; Hu, Y.; Sampson, N. S.; Zucker, S.; Cao, J. *J. Biol. Chem.* **2011**, *286*, 33167−33177.

(2) Hu, J.; Van den Steen, P. E.; Sang, Q.-X. A.; Opdenakker, G. *Nat. Rev. Drug Discovery* **2007**, *6*, 480−498.

(3) Vandenbroucke, R. E.; Libert, C. *Nat. Rev. Drug Discovery* **2014**, *13*, 904−927.

(4) Chung, E. Y.; Ochs, C. J.; Wang, Y.; Lei, L.; Qin, Q.; Smith, A. M.; Strongin, A. Y.; Kamm, R.; Qi, Y.-X.; Lu, S.; Wang, Y. *Nano Lett.* **2015**, *15*, 5025−5032.

(5) Didenko, V. V. *BioTechniques* **2001**, *31*, 1106−1121.

(6) Wu, L.; Huang, C.; Emery, B. P.; Sedgwick, A. C.; Bull, S. D.; He, X.-P.; Tian, H.; Yoon, J.; Sessler, J. L.; James, T. D. *Chem. Soc. Rev.* **2020**, *49*, 5110−5139.
(7) Meng, F.; Sachs, F. *J. Cell Sci.* **2012**, *125*, 743−750.
(8) Zheng, J.; Yang, R.; Shi, M.; Wu, C.; Fang, X.; Li, Y.; Li, J.; Tan, W. *Chem. Soc. Rev.* **2015**, *44*, 3036−3055.
(9) Lakowicz, J. R. *Principles of Fluorescence spectroscopy*, 3rd ed.; Springer: New York, 2006; p 954.
(10) Bruchez, M.; Moronne, M.; Gin, P.; Weiss, S.; Alivisatos, A. P. *Science* **1998**, *281*, 2013−2016.
(11) Mattoussi, H.; Mauro, J. M.; Goldman, E. R.; Anderson, G. P.; Sundar, V. C.; Mikulec, F. V.; Bawendi, M. G. *J. Am. Chem. Soc.* **2000**, *122*, 12142−12150.
(12) Peng, X. *Nano Res.* **2009**, *2*, 425−447.
(13) Medintz, I. L.; Mattoussi, H. *Phys. Chem. Chem. Phys.* **2009**, *11*, 17−45.
(14) Nan, W.; Niu, Y.; Qin, H.; Cui, F.; Yang, Y.; Lai, R.; Lin, W.; Peng, X. *J. Am. Chem. Soc.* **2012**, *134*, 19685−19693.
(15) Hanifi, D. A.; Bronstein, N. D.; Koscher, B. A.; Nett, Z.; Swabeck, J. K.; Takano, K.; Schwartzberg, A. M.; Maserati, L.; Vandewal, K.; Burgt, Y. v. d.; Salleo, A.; Alivisatos, A. P. *Science* **2019**, *363*, 1199−1202.
(16) Hildebrandt, N.; Spillmann, C. M.; Algar, W. R.; Pons, T.; Stewart, M. H.; Oh, E.; Susumu, K.; Díaz, S. A.; Delehanty, J. B.; Medintz, I. L. *Chem. Rev.* **2017**, *117*, 536−711.
(17) Freeman, R.; Willner, I. *Chem. Soc. Rev.* **2012**, *41*, 4067−4085.
(18) Medintz, I. L.; Uyeda, H.; Goldman, E.; Mattoussi, H. *Nat. Mater.* **2005**, *4*, 435−446.
(19) Clapp, A. R.; Medintz, I. L.; Mauro, J. M.; Fisher, B. R.; Bawendi, M. G.; Mattoussi, H. *J. Am. Chem. Soc.* **2004**, *126*, 301−310.
(20) Michalet, X.; Pinaud, F.; Bentolila, L.; Tsay, J.; Doose, S.; Li, J.; Sundaresan, G.; Wu, A.; Gambhir, S.; Weiss, S. *Science* **2005**, *307*, 538−544.
(21) Mattoussi, H.; Palui, G.; Na, H. B. *Adv. Drug Delivery Rev.* **2012**, *64*, 138−166.
(22) Jin, Z.; Kapur, A.; Wang, W.; Hernandez, J. D.; Thakur, M.; Mattoussi, H. *J. Chem. Phys.* **2019**, *151*, No. 164703.
(23) Murray, C. B.; Norris, D. J.; Bawendi, M. G. *J. Am. Chem. Soc.* **1993**, *115*, 8706−8715.
(24) Dabbousi, B. O.; RodriguezViejo, J.; Mikulec, F. V.; Heine, J. R.; Mattoussi, H.; Ober, R.; Jensen, K. F.; Bawendi, M. G. *J. Phys. Chem. B* **1997**, *101*, 9463−9475.
(25) Talapin, D. V.; Lee, J. S.; Kovalenko, M. V.; Shevchenko, E. V. *Chem. Rev.* **2010**, *110*, 389−458.
(26) Clapp, A. R.; Goldman, E. R.; Mattoussi, H. *Nat. Protoc.* **2006**, *1*, 1258−1266.
(27) Mahler, B.; Spinicelli, P.; Buil, S.; Quelin, X.; Hermier, J. P.; Dubertret, B. *Nat. Mater.* **2008**, *7*, 659−664.
(28) Ma, L.; Tu, C.; Le, P.; Chitoor, S.; Lim, S. J.; Zahid, M. U.; Teng, K. W.; Ge, P.; Selvin, P. R.; Smith, A. M. *J. Am. Chem. Soc.* **2016**, *138*, 3382−3394.
(29) Uyeda, H. T.; Medintz, I. L.; Jaiswal, J. K.; Simon, S. M.; Mattoussi, H. *J. Am. Chem. Soc.* **2005**, *127*, 3870−3878.
(30) Muro, E.; Pons, T.; Lequeux, N.; Fragola, A.; Sanson, N.; Lenkei, Z.; Dubertret, B. *J. Am. Chem. Soc.* **2010**, *132*, 4556−4557.
(31) Wang, W.; Ji, X.; Kapur, A.; Zhang, C.; Mattoussi, H. *J. Am. Chem. Soc.* **2015**, *137*, 14158−14172.
(32) Wang, W.; Kapur, A.; Ji, X.; Safi, M.; Palui, G.; Palomo, V.; Dawson, P. E.; Mattoussi, H. *J. Am. Chem. Soc.* **2015**, *137*, 5438−5451.
(33) Tasso, M.; Giovanelli, E.; Zala, D.; Bouccara, S.; Fragola, A.; Hanafi, M.; Lenkei, Z.; Pons, T.; Lequeux, N. *ACS Nano* **2015**, *9*, 11479−11489.
(34) Susumu, K.; Mei, B. C.; Mattoussi, H. *Nat. Protoc.* **2009**, *4*, 424−436.
(35) Jokerst, J. V.; Lobovkina, T.; Zare, R. N.; Gambhir, S. S. *Nanomedicine* **2011**, *6*, 715−728.
(36) Jin, Z.; Yeung, J.; Zhou, J.; Cheng, Y.; Li, Y.; Mantri, Y.; He, T.; Yim, W.; Xu, M.; Wu, Z.; Fajtova, P.; Creyer, M. N.; Moore, C.; Fu, L.; Penny, W. F.; O'Donoghue, A. J.; Jokerst, J. V. *Chem. Mater.* **2022**, *34*, 1259−1268.
(37) Jin, Z.; Sugiyama, Y.; Zhang, C.; Palui, G.; Xin, Y.; Du, L.; Wang, S.; Dridi, N.; Mattoussi, H. *Chem. Mater.* **2020**, *32*, 7469−7483.
(38) Palui, G.; Aldeek, F.; Wang, W.; Mattoussi, H. *Chem. Soc. Rev.* **2015**, *44*, 193−227.
(39) Shen, H.; Jawaid, A. M.; Snee, P. T. *ACS Nano* **2009**, *3*, 915−923.
(40) Bartczak, D.; Kanaras, A. G. *Langmuir* **2011**, *27*, 10119−10123.
(41) Aldeek, F.; Safi, M.; Zhan, N. Q.; Palui, G.; Mattoussi, H. *ACS Nano* **2013**, *7*, 10197−10210.
(42) Sapsford, K. E.; Pons, T.; Medintz, I. L.; Higashiya, S.; Brunel, F. M.; Dawson, P. E.; Mattoussi, H. *J. Phys. Chem. C* **2007**, *111*, 11528−11538.
(43) Palui, G.; Avellini, T.; Zhan, N.; Pan, F.; Gray, D.; Alabugin, I.; Mattoussi, H. *J. Am. Chem. Soc.* **2012**, *134*, 16370−16378.
(44) Liu, Y.; Le, P.; Lim, S. J.; Ma, L.; Sarkar, S.; Han, Z.; Murphy, S. J.; Kosari, F.; Vasmatzis, G.; Cheville, J. C.; Smith, A. M. *Nat. Commun.* **2018**, *9*, No. 4461.
(45) Aldeek, F.; Hawkins, D.; Palomo, V.; Safi, M.; Palui, G.; Dawson, P. E.; Alabugin, I.; Mattoussi, H. *J. Am. Chem. Soc.* **2015**, *137*, 2704−2714.
(46) ten Hove, J. B.; Schijven, L. M. I.; Wang, J.; Velders, A. H. *Chem. Commun.* **2018**, *54*, 13355−13358.
(47) Mishra, D.; Wang, S.; Michel, S.; Palui, G.; Zhan, N.; Perng, W.; Jin, Z.; Mattoussi, H. *Phys. Chem. Chem. Phys.* **2018**, *20*, 3895−3902.
(48) Zhan, N.; Palui, G.; Mattoussi, H. *Nat. Protoc.* **2015**, *10*, 859−874.
(49) Hermanson, G. T. *Bioconjugate Techniques*, 3rd ed.; Academic Press: London, 2013.
(50) Zhan, N.; Palui, G.; Merkl, J.-P.; Mattoussi, H. *J. Am. Chem. Soc.* **2016**, *138*, 3190−3201.
(51) Zhang, C.; Palui, G.; Zeng, B.; Zhan, N.; Chen, B.; Mattoussi, H. *Chem. Mater.* **2018**, *30*, 3454−3466.
(52) Vashist, S. K. *Diagnostics* **2012**, *2*, 23−33.
(53) Lichte, A.; Kolkenbrock, H.; Tschesche, H. *FEBS Lett.* **1996**, *397*, 277−282.
(54) Medintz, I. L.; Clapp, A. R.; Brunel, F. M.; Tiefenbrunn, T.; Uyeda, H. T.; Chang, E. L.; Deschamps, J. R.; Dawson, P. E.; Mattoussi, H. *Nat. Mater.* **2006**, *5*, 581−589.
(55) Boeneman, K.; Mei, B. C.; Dennis, A. M.; Bao, G.; Deschamps, J. R.; Mattoussi, H.; Medintz, I. L. *J. Am. Chem. Soc.* **2009**, *131*, 3828−3829.
(56) Algar, W. R.; Malonoski, A.; Deschamps, J. R.; Blanco-Canosa, J. B.; Susumu, K.; Stewart, M. H.; Johnson, B. J.; Dawson, P. E.; Medintz, I. L. *Nano Lett.* **2012**, *12*, 3793−3802.
(57) Jin, Z.; Dridi, N.; Palui, G.; Palomo, V.; Jokerst, J. V.; Dawson, P. E.; Sang, Q.-X. A.; Mattoussi, H. Evaluating the Catalytic Efficiency of the Human Membrane-Type 1 Matrix Metalloproteinase (MMP-14) Using AuNP−Peptide Conjugates *J. Am. Chem. Soc.* **2023**, in press, DOI: 10.1021/jacs.2c12032.
(58) Moroz, P.; Jin, Z.; Sugiyama, Y.; Lara, D. A.; Razgoniaeva, N.; Yang, M.; Kholmicheva, N.; Khon, D.; Mattoussi, H.; Zamkov, M. *ACS Nano* **2018**, *12*, 5657−5665.
(59) Förster, T. *Ann. Phys.* **1948**, *437*, 55−75.
(60) Chou, K. F.; Dennis, A. M. *Sensors* **2015**, *15*, 13288−13325.
(61) Ji, X.; Wang, W.; Mattoussi, H. *Phys. Chem. Chem. Phys.* **2015**, *17*, 10108−10117.
(62) Kridel, S. J.; Sawai, H.; Ratnikov, B. I.; Chen, E. I.; Li, W.; Godzik, A.; Strongin, A. Y.; Smith, J. W. *J. Biol. Chem.* **2002**, *277*, 23788−23793.
(63) Neumann, U.; Kubota, H.; Frei, K.; Ganu, V.; Leppert, D. *Anal. Biochem.* **2004**, *328*, 166−173.
(64) Dietz, M. S.; Wehrheim, S. S.; Harwardt, M.-L. I. E.; Niemann, H. H.; Heilemann, M. *Nano Lett.* **2019**, *19*, 8245−8249.
(65) Mattoussi, H.; Cumming, A. W.; Murray, C. B.; Bawendi, M. G.; Ober, R. *Phys. Rev. B* **1998**, *58*, 7850−7863.

https://doi.org/10.1021/acs.analchem.2c03400
Anal. Chem. 2023, 95, 2713−2722

(66) Jin, Z.; Mantri, Y.; Retout, M.; Cheng, Y.; Zhou, J.; Jorns, A.; Fajtova, P.; Yim, W.; Moore, C.; Xu, M.; Creyer, M. N.; Borum, R. M.; Zhou, J.; Wu, Z.; He, T.; Penny, W. F.; O'Donoghue, A. J.; Jokerst, J. V. *Angew. Chem., Int. Ed.* **2022**, *61*, No. e202112995.
(67) Johnson, B. J.; Russ Algar, W.; Malanoski, A. P.; Ancona, M. G.; Medintz, I. L. *Nano Today* **2014**, *9*, 102−131.
(68) Claussen, J. C.; Malanoski, A.; Breger, J. C.; Oh, E.; Walper, S. A.; Susumu, K.; Goswami, R.; Deschamps, J. R.; Medintz, I. L. *J. Phys. Chem. C* **2015**, *119*, 2208−2221.
(69) Tzafriri, A. R. *Bull. Math. Biol.* **2003**, *65*, 1111−1129.
(70) Díaz, S. A.; Sen, S.; Boeneman Gemmill, K.; Brown, C. W.; Oh, E.; Susumu, K.; Stewart, M. H.; Breger, J. C.; Lasarte Aragonés, G.; Field, L. D.; Deschamps, J. R.; Král, P.; Medintz, I. L. *ACS Nano* **2017**, *11*, 5884−5896.
(71) Hurst, D. R.; Schwartz, M. A.; Jin, Y.; Ghaffari, M. A.; Kozarekar, P.; Cao, J.; Sang, Q. X. *Biochem. J.* **2005**, *392*, 527−536.
(72) Segel, L. A. *Bull. Math. Biol.* **1988**, *50*, 579−593.
(73) Armbruster, D. A.; Pry, T. *Clin. Biochem. Rev.* **2008**, *29*, S49−S52.
(74) Schurr, J. M. *Biophys. J.* **1970**, *10*, 717−727.
(75) Xu, F.; Ding, H. *Appl. Catal., A* **2007**, *317*, 70−81.
(76) Wu, C.-S.; Lee, C.-C.; Wu, C.-T.; Yang, Y.-S.; Ko, F.-H. *Chem. Commun.* **2011**, *47*, 7446−7448.

https://doi.org/10.1021/acs.analchem.2c03400
Anal. Chem. 2023, 95, 2713−2722